Dalton Transactions

An international journal of inorganic chemistry

Accepted Manuscript

ROYAL SOCIETY OF CHEMISTRY

rsc.li/dalton

ROYAL SOCIETY OF CHEMISTRY View Article Online
DOI: 10.1039/C9DT02890K

Journal Name

ARTICLE

Monitoring Fragmentation and Oligomerization of A di-μ-methoxo Bridged Copper(II) Complex: Structure, Mass Spectrometry, Magnetism and DFT Studies

Received 00th January 20xx,
Accepted 00th January 20xx

DOI: 10.1039/x0xx00000x

www.rsc.org/

Xing-Xing Shi,[a,+] Qiu-Jie Chen,[b,+] Xue-Li Chen,[a] Yuexing Zhang,[*,b] Mohamedally Kurmoo,[c] Ming-Hua Zeng*[,a,b]

Analyses of the structural information of molecular fragments from the mass spectra of the solid-state products and their reaction solutions allow for the understanding of their formations and of their diverse properties. The reaction of $CuCl_2$ and 1-methyl-1H-benzo[*d*]imidazol-2-yl)methanol (H*L*) led only to crystals containing molecular dimers of $[Cu_2(L)_2Cl_2]$ (**Cu2**). The Cu^{II}–Cu^{II} distance and Cu–OR–Cu angle in the structure are 3.044 Å and 104.8°, respectively. The magnetic susceptibility (3–400 K) is characterized by a very strong intradimer antiferromagnetic interaction of J = -465 and interdimer zj = -0.83 cm^{-1}. But mass spectrometry of a dissolved single crystal in different source energies identifies both its fragmentation and oligomerization to $[Cu^{II}_3]$ and $[Cu^{II}_4]$. DFT calculations give the relative stabilization energies of the fragments observed in ESI-MS to provide a formation process.

Introduction

There is currently major interest in coordination clusters for their syntheses, beautiful structures and rich functions.[1] The design of structures and functions of the coordination compounds has been pursuing one goal irrespective of whether they are complex networks, multi-nuclear clusters, and even mononuclear compounds. In this respect, planar coordination complexes are preferable to form electronic bands because they can stack on top of each other, thus providing considerable overlap of the d_z^2 orbitals. Such systems have been subjects of interest in the field of molecular conductors, superconductors and magnets.[2] While there is importance in their solid-state properties, their solubility and stability in solution are as important for exploiting other functions,[3] such as fluorescence in bioactivity and magnetism.[4] The ESI-MS technique has become important in studying the stability of clusters and their solution behaviors. Furthermore, the structure of the cluster in the solid state and the fragments existing in solution from the reaction allow the assembly mechanism to be deduced.[5] Though these mechanisms are quite complex, certain advances have been made, for example in 3d-metal coordination clusters, polyoxometalates, and coordination cages.[4b,6] Here, we take advantage of the early knowledge of ESI-MS that our research has identified which include several interesting behaviors, for example: exchange/elimination of inner bridging ligands, ion-trapping, rearrangements, recognition of clusters;[7] building blocks in the assembly process of Co_{16} and Zn_{14} clusters;[7a,8] assembly and competition of ligands is revealed for coordination clusters constructed from two different shaped ligands by ESI-MS and confirm the mechanism of competition and transformation among different species of Co_4 clusters.[9] In our previous works, we successfully applied mass spectrometry to study mononuclear compound $Cu(L)Cl_2$, (**Cu1**), which indicates the occurrence of several chemical processes, viz. fragmentation of the ligand, oligomerization, and redox reaction of alcohol to aldehyde and Cu^{II} to Cu^{I}.[10]

Here, we take advantage of the early knowledge about **Cu1** system to further explore the formation of the $[Cu^{II}(L)Cl]_2$ complex, here labeled as **Cu2** (Figure 1). We found a very unusual chemistry in the MS whereby in addition to smaller fragmented species larger ones than the parent crystalline compound was observed. Moreover, the research focus of a series of rich changes about the binuclear copper complexes under mass spectrometry in different source voltages and their potential guiding significance in the

[a] *Key Laboratory for the Chemistry and Molecular Engineering of Medicinal Resources School of Chemistry and Pharmaceutical Sciences, Guangxi Normal University, Guilin, 541004, P. R. China. E-mail: zmh@mailbox.gxnu.edu.cn*

[b] *Hubei Collaborative Innovation Center for Advanced Organic Chemical Materials, Ministry of Education Key Laboratory for the Synthesis and Application of Organic Functional Molecules, College of Chemistry and Chemical Engineering, Hubei University, Wuhan, 430062, P. R. China. E-mail: zhangyuexing@sdu.edu.cn.*

[c] *Université de Strasbourg, Institut de Chimie de Strasbourg, CNRS-UMR7177, 4 rue Blaise Pascal, Strasbourg Cedex 67070, France.*

[+] *These authors contributed equally to this work.*

Electronic Supplementary Information (ESI) available. See DOI: 10.1039/x0xx00000x

View Article Online
DOI: 10.1039/C9DT02800K

syntheses of high nuclear compounds. In solution, the simple dinuclear species is always the building unit of final products, which is also the preliminary reactant of the assembly process. In addition, the magnetic susceptibility indicates strong antiferromagnetic interaction, which are well clarified by the theoretical simulation. Here, we present a study of the crystallography, DFT, mass spectrometry and magnetic property. Understanding the stability, intermolecular interaction, geometry distortion, integration, cleavage of dinuclear species would build a crucial base for the mechanism study of polynuclear clusters.

Results and discussion

Crystal Structure. X-ray diffraction data reveal that Cu2 crystallizes in the triclinic space group *P*-1 (Tables S1-2). In its structure, the Cu^{2+} exhibits square-planar coordination geometry with one terminal Cl, N and O atoms from the chelating-bridging L (Figure 1a). The coordination geometry for Cu^{2+} in an asymmetric unit was performed by continuous-shape measurements (*CShM*) using SHAPE 2.0 software[11] (Table S3), which demonstrates the Cu_2O_2 core being almost planar (angle between OCuO planes of 0.000(2)°).[12] The Cu1···Cu1' distance is 3.044 Å, and the Cu1–O1–Cu1' angle is 104.8°. Numerous dinuclear Cu(II) compounds with alkoxido-bridging ligands and a planar geometry around the Cu(II) ions have been reported in the literature (Table S4). The calculation of the deviation of the bond length of the low-temperature structure shows that the structure at low temperature varies little compared to the room temperature (Table S5). So, the low temperature magnetic data could still be analyzed with the structural data acquired at room temperature.[13]

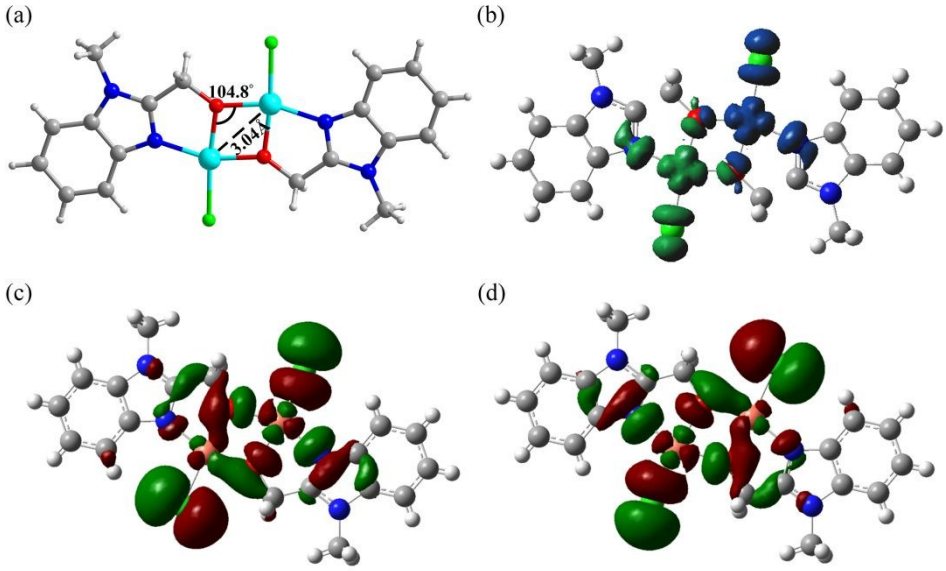

Figure 1. (a) Perspective views of the coordination environment of Cu2. Symmetry codes: 2-x, -y, 1-z. Color code: Cu, turquiose; Cl, bright green; O, red; N, blue; C, gray. (b) The calculated spin density distribution using B3LYP for the broken symmetry state. (c) Molecular orbital distribution in α-direction and (d) β-direction of the high spin state.

There is one H-bond to link the dimeric complex into one-dimensional chains (Figure S4). There is C(Me)–H···Cl, where C···Cl is 3.724 Å (∠ CHCl = 164.1°). There are two Cu···π stacking interactions between pairs of benzene or imidazole (Ph or C3N2) rings - centroid-to-centroid distance of 3.437 and 3.446 Å. A moderate C–H···π(Ph) interaction exists where the distance from C(Me) to the nearest benzene ring are 3.906 Å and angle is 147.7°. The Cu···π and C–H···π interactions may be responsible for weak magnetic coupling (Table S6).[14] To qualitatively describe the above interactions, complexation energies between **Cu2** molecules were calculated using the DFT method. Computed energies for several models are listed in Table S6. It is found that the supramolecular interactions,[15] Cu···π(C3N2), Cu···π(Ph) overlap between triazole rings, and C(Me)–H···Cl H-bond, have very large complexation energies lying in the range of -10 – -43 kcal/mol. Meanwhile it is found that the C-H···Cl H-bond and C(Me)-H···π(PhC_3N_2) interaction have marginally lower complexation energies (-10 – -12 kcal/mol). These results indicate that the dominating intermolecular interaction is Cu ··π interaction.

Magnetic Properties. The magnetization measurements were performed on a MPMS SQUID magnetometer in the temperature range of 3–400 K and field range ±50 kOe. The plot of $\chi_m T$ *vs T* for **Cu2** is shown in Figure 2. At 400 K the $\chi_m T$ product has a value of 0.097 $cm^3\ mol^{-1}\ K$, which is far below the value for two non-interacting Cu(II) ions (0.75 $cm^3\ mol^{-1}\ K$, assuming g = 2). From 400 K the $\chi_m T$ product decreases rapidly to a value of 0.003 $cm^3\ mol^{-1}\ K$ below 100 K. This susceptibility behavior indicates strong antiferromagnetic interaction.[16] The best fit for the whole data set was obtained with J = -465 cm^{-1}, g = 2.20, mean-field zj = -0.83 cm^{-1} using the PHI program. The magnetization at 2 K reaches only 0.93 μ_B per dimer which is less than the expected 3.46 μ_B confirming the strong coupling between copper centers. The large coupling

correlates well with existing its dependence on the Cu−O−Cu angle of 104.8° (Table S4).

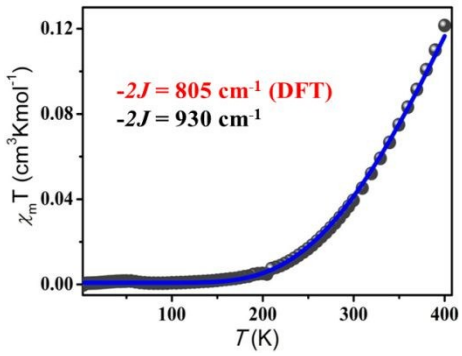

Figure 2. Temperature dependence of $\chi_m T$ vs T for **Cu2**. Solid lines are the theoretical calculation.

Data from the variable-temperature magnetic susceptibility (3–400 K) indicate that the magnetic moment is almost zero from 3 to 200 K, indicating a very strong antiferromagnetic coupling between the bridged Cu(II) ions and the binuclear complex has a singlet state. To elucidate the magnetic exchange and confirm the experimental result, DFT calculations were performed on **Cu2**. The calculations are based on binuclear Cu(II) Hamiltonian ($\hat{H} = -2J\hat{S}_{Cu}\hat{S}_{Cu}$) and Noodleman's suggestions.[17] The magnetic coupling constant for a binuclear Cu(II) system can be obtained using the expression $E_T - E_{BS} = -2J$ (E_T = -2381.63248351 au, E_{BS} = -2381.63615391 au), where E_T and E_{BS} represent the energies of triplet and broken-symmetry singlet states, respectively. The energy difference value between the singlet and triplet states is calculated as $-2J$ = 805 cm^{-1}. The large 2J will stabilize the complex in a singlet state at low temperature, in agreement with experimental results.

The magnetic exchange could be explained by spin density distribution and orbital analysis. Figure 1 (b-d) shows the calculated spin density distribution, magnetic molecular orbital (HOMO-1) distribution in α- and β-direction using B3LYP for the broken symmetry singlet state. In order to investigate the magnetic exchange, clearly indicating that the antiferromagnetic interaction between the H*L*-bridged binuclear Cu(II) ions is due to large overlap of the Cu(II) $3d_{x2-y2}$ orbitals and the bridging O p_y orbitals. For extended Jahn-Teller axially distorted Cu(II), they generally have the one unpaired electron in the $3d_{x2-y2}$ orbital based on the calculated spin density distribution of some atoms for the broken-symmetry singlet state (Table S7). However, theoretically, the total spin on Cu(II) is only 0.6. Also, the atoms coordinated to Cu(II) exhibit the same sign as Cu(II), suggesting significant spin delocalization for Cu(II). For O atoms of H*L* bridging ligands, spin densities are very small due to two Cu(II) ions simultaneously delocalizing to the ligands, which results in very small spin density on oxygen.

Electrospray Ionization Mass Spectrometry. It has already been observed the formation of dimers in mass spectrometry under high voltages of the monomeric **Cu1** compound.[10] The solvothermal reaction under the present conditions led single crystals having the binuclear structure. This discovery suggests that the study of low nuclearity compound can be converted to higher nuclearity fragment. The crystals of **Cu2** were dissolved in DMSO and diluted with CH_3OH and the MS spectra were recorded in positive mode. (Figure S5-6 Table S8). Interestingly, we found that a series of chemical changes, such as cleavage, assembly, redox and so on have been observed. Compared to **Cu1**, there are more abundant fragments. Theoretical calculations show that the Gibbs free energy of **Cu2** of active fragment of $[Cu(L)]^+$ is 384 kcal/mol lower than that of **Cu1** 477 kcal/mol.[10] We conjecture that **Cu2** is a post-synthetic modified precursor with more potential than **Cu1**.

View Article Online
DOI: 10.1039/C9DT02890H

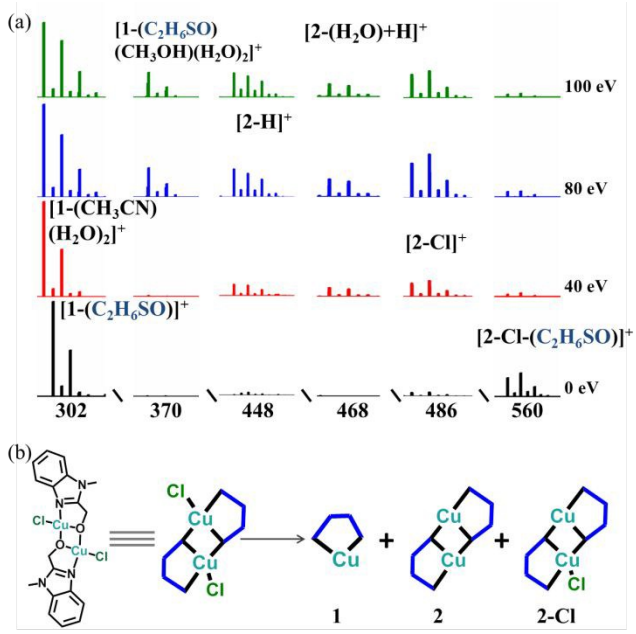

Figure 3. (a) Positive mode ESI-MS of Cu2, the area presents the split species; (b) The Chemdraw model for predicted structures of Cu2 split to MS fragments.

Under in-source energy of 0 eV, the dominant peak in the positive mode spectrum was found at *m/z* of 302.01 $[Cu^{II}(L)(C_2H_6SO)]^+$ ($[1\text{-}(C_2H_6SO)]^+$) indicates the molecular unit forming the crystal is unstable in solution (Figure 3). Moreover, the solution also contains other fragments, $[Cu^{II}(L)Cl(C_2H_6SO)+H]^+$ (calc. 337.99), $[Cu^{II}(L)(C_2H_6SO)_2]^+$ (calc. 380.03), $[Cu^{II}(L)_2+H]^+$ (386.08), $[Cu^{II}_4(L)_4Cl_3]^+$ ($[4\text{-}4Cl_3]^+$) (calc. 1004.91). And, more remarkable, some fragment peaks relative intensity is less than ten percent, for instance $[Cu^{II}_2(L)_2Cl]^+$ (calc. 484.97), $[KCu^{I}Cu^{II}(L)_2Cl(OH)]^+$ (calc. 540.91), $[Cu^{II}_2(L)_2Cl(C_2H_6SO)]$+ (calc. 562.98) show parental units. Under in-source energy of 40, 80, 100 eV, the MS show different solvated monomeric fragments, $[Cu^{II}(L)(CH_3CN)(H_2O)_2]^+$ ($[1\text{-}(CH_3CN)(H_2O)_2]^+$) (calc. 301.05), $[Cu^{I}(L)(C_2H_6SO)(CH_3OH)(H_2O)_2]^+$ ($[1\text{-}(C_2H_6SO)(CH_3OH)(H_2O)_2]^+$) (calc. 369.09), dimeric fragments, $[Cu^{II}_2(L)_2\text{-}H]^+$ ($[2\text{-}H]^+$) (calc. 446.99), $[Cu^{I}_2(L)_2(H_2O)+H]^+$ ($[2\text{-}(H_2O)+H]^+$) (calc. 467.02) and $[Cu^{II}_2(L)_2Cl]^+$ ($[2\text{-}Cl]^+$) (calc. 484.97) and most importantly, oligomeric fragments $[Cu^{II}_3(L)_3Cl_2]^+$ ($[3]^+$) (calc. 743.94), $[Cu^{I}_2Cu^{II}_2(L)_3Cl_2(H_2O)]^+$ ($[4\text{-}3Cl_2\text{-}(H_2O)]^+$) (calc. 824.88), $[Cu^{II}_4(L)_3Cl_3(CH_3O)(CH_3OH)]^+$ ($[4\text{-}3Cl_3\text{-}(CH_3O)(CH_3OH)]^+$) (calc. 904.88) and $[Cu^{II}_4$ $(L)_3Cl_4(H_2O)(CH_3OH)]^+$ ($[4\text{-}3Cl_4\text{-}(H_2O)(CH_3OH)]^+$) (calc. 928.84). While the intensity of $[Cu^{II}(L)(C_2H_6SO)]^+$ (calc. 302.01) gradually decreases those of $[Cu^{II}(L)(CH_3CN)(H_2O)_2]^+$ (calc. 301.05)

and $[Cu^{I}(L)(H_2O)_2+H]^+$ (calc. 369.09) gradually increase and $[Cu^{II}_2(L)_2Cl(C_2H_6SO)]^+$ ($[2\text{-}Cl\text{-}(C_2H_6SO)]^+$) (calc. 562.98) frame gradually disappear under in-source energy of 0 eV. Although we cannot obtain crystals of these fragments by purification techniques, we can still theoretically simulate their molecular structures using literature search results,[19] (Figure 4) which are usually dinuclear unit bridged by μ_2-O and μ_2-Cl, tetranuclear defected cubane bridged by μ_3-O and μ_2-Cl.

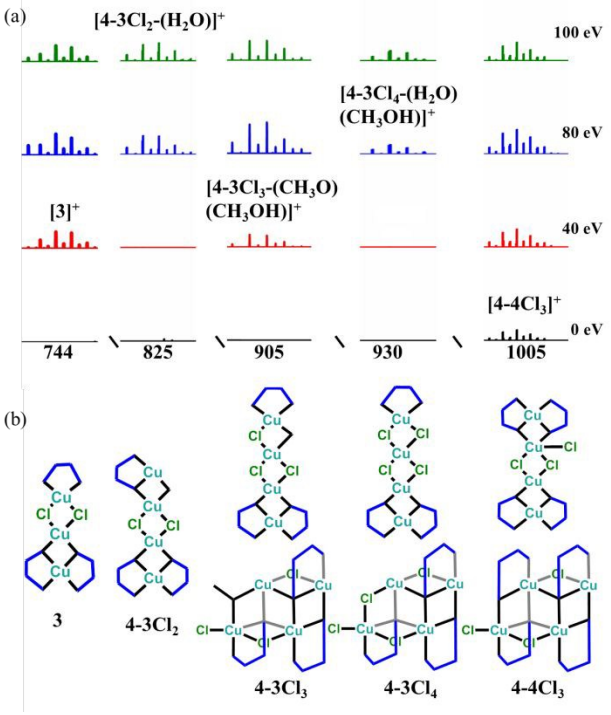

Figure 4. Positive mode ESI-MS of **Cu2**. (a) The area presents the oligomerization from $[Cu_3]$ to $[Cu_4]$. The peak intensity in the region of *m/z* > 700 has been amplified for clarity. (b) The Chemdraw models for predicted structures of **Cu2** split to MS fragments**.**

According to the typical composition of peaks of the MS spectra, the possible structures of fragments are fully optimized and their corresponding forming Gibbs free energies were calculated. The fact obtained from MS that peaks for $[Cu^{II}(L)]^+$ and $[Cu^{II}_2(L)_2Cl]^+$ appear at in-source energy of 0 eV indicates the formation of $[Cu^{II}(L)]^+$ and $[Cu^{II}_2(L)_2Cl]^+$ is not so hard in MS condition despite of the very large positive Gibbs free energy change of 384 and 329 kcal/mol. Once $[Cu^{II}(L)]^+$ and $[Cu^{II}_2(L)_2Cl]^+$ are formed, the formation of fragments 5-9 is straightforward with negative Gibbs free energy changes (Figure 5). The Gibbs free energy changes for the reactions are:

-586 kcal/mol: $2[Cu(L)]^+ + CuCl_2 + L \rightarrow 5$

-507 kcal/mol: $2[Cu(L)]^+ + 2CuCl^- + H_2O + L \rightarrow 6$

-343 kcal/mol: $2[Cu(L)]^+ + CuCl_2 + CuCl^- + CH3O^- + L \rightarrow 7\text{-}1$

-754 kcal/mol: $2[Cu(L)]^+ + 2L + CuCl_2 + CuCl^- \rightarrow 9\text{-}2$

-483 kcal/mol: $[Cu_2(L)Cl]^+ + [Cu(L)Cl]^- + CuCl_2 \rightarrow 8\text{-}1$

-613 kcal/mol: $2[Cu(L)]^+ + 2CuCl_2 + L \rightarrow 8\text{-}2$

-397 kcal/mol: $[Cu_2(L)_2Cl]^+ + CuCl^- + [Cu(L)]^+ + H_2O \rightarrow 9\text{-}1$.

Importantly, the optimized fragments 1-9 all have negative HOMO orbital energies and have no imaginary frequency (Table S9-10), indicating the proposed structures obtained from peaks of the MS spectra assigned based on the *m/z* values and isotopic distributions with the help of single-crystal structure is reasonable and stable. We conjectured the possible structures of the fragments 7-9 by CCDC and theoretical calculations, combined with the value of Gibbs free energies and the order in which it appeared in the pressurized mass spectrometry. We can speculate that the order of the Gibbs free energies is 9 > 5 (-586) ~ 7(-601) > 6~8, and then the most probable unique structural formula can be determined, which are $[Cu^{II}_4(L)_3Cl_3(CH_3OH)\text{-}H]^+$ (calc. 904.88) is 7-1, $[Cu^{II}_4(L)_3Cl_4(H_2O)(CH_3OH)]^+$ (calc. 928.84) is 8-1 and $[Cu^{II}_4(L)_4Cl_3]^+$ (calc. 1004.91) is 9-2. For the first time, we combine the Gibbs free energy with the order in which mass spectrometry occurs to identify more likely structures (Figure 5).

View Article Online
DOI: 10.1039/C9DT02890K

Journal Name

ARTICLE

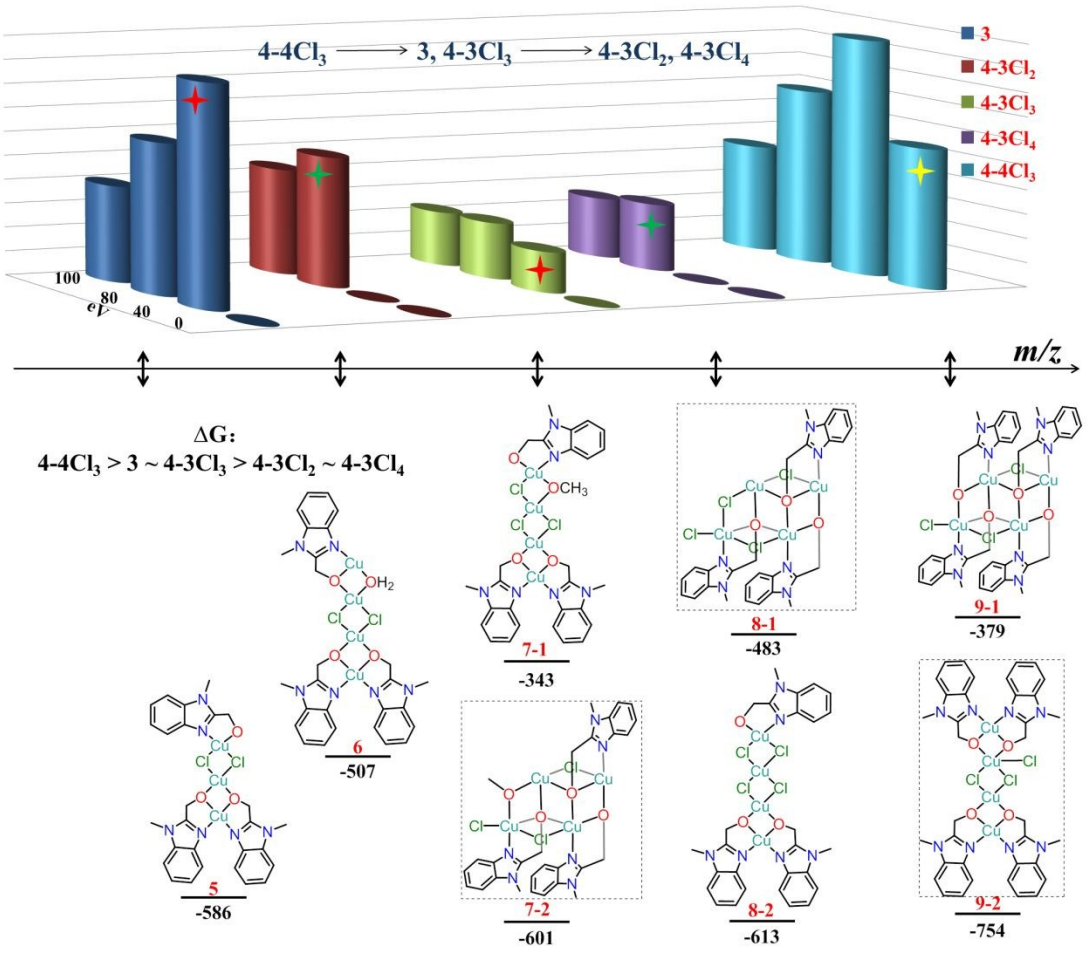

Figure 5. Top: Positive mode ESI-MS of **Cu2**. The predicted structures of the MS fragments (red number) from **Cu2**, the calculated Gibbs free energy changes (ΔG, black number, in kcal mol^{-1}), having crystal structure (solid line box), and guessing the most likely structure (dotted box). Bottom: The trend that the relative intensity of 5-9 fragments with the different voltages (0, 40, 80, 100 eV).

Conclusions

In summary, the novel planar dinuclear compound with $[Cu_2(L)_2Cl_2]$ has been synthesized by solvothermal reactions. The Cu–O–Cu angle for the compound of **Cu2** is 104.8° and according to the correlation formula a value of -402.5 cm^{-1} would be predicted, which fits well the observed value of -465 cm^{-1}. The above result also confirmed by combining the experimental fitting and theoretical calculations approach strictly that **Cu2** exhibits a stronger antiferromagnetic behavior. The fragmentation and oligomerization processes of the compound monitored by ESI-MS at variable in-source energies were performed on solutions of the crystals. Meanwhile, DFT and literature search results highlighted these MS fragments exist. The more likely structures of fragments were determined by combined with DFT and MS method for the first time, which open new way to more clearly verify the structure information obtained from MS spectra and would be greatly helpful for the study of similar systems. It prompted us to have a new understanding of mass spectrometry and enriched the application of MS. It is believed the findings will benefit rational design and construction of coordination compounds with targeted magnetic properties in the future.

Experimental Section

Materials and Measurements: All the reagents were obtained from commercial sources and used without further purification.

View Article Online
DOI: 10.1039/C9DT02890K

Elemental analyses for C, H, and N were performed on a Vario Micro Cube. Thermogravimetric analyses (TGA) were performed in a flow of nitrogen at a heating rate of 10 °C/min using a NETZSCH TG 209 F3. Infrared spectra of **Cu2** were recorded by transmission through KBr pellets containing ca. 0.5% of the compound using a PE Spectrum FT-IR spectrometer (400-4000 cm^{-1}). Powder X-ray diffraction (PXRD) intensities were measured at 296 K on a Rigaku D/max-IIIA diffractometer (Cu Kα). The crystalline powder sample was prepared by crushing the crystals, and scan of 3 to 60° was recorded at a rate of 5° min^{-1}. Calculated diffraction pattern of the compound was generated using the Mercury 3.9 software.[20] Magnetic properties of polycrystalline sample was measured in the temperature range of 3-400 K.

Synthesis of Cu2: $CuCl_2{\cdot}2H_2O$ (170 mg, 1 mmol) and H*L* (81 mg, 0.5 mmol) and methanol (15 mL) were stirred for 30 minutes and then placed in a Teflon-lined steel bomb which is kept at 100 °C for 2 day. The autoclave was then cooled at a rate of 10 °C·h^{-1}, and the blue crystals of $[Cu(L)Cl]_2$ (**Cu2**) were collected, washed with MeOH and dried in air (Figure S1). The yield slightly varies for each batch even under similar condition. There was no solvent in the structure of **Cu2**, which was confirmed by thermogravimetric and elemental analyses (EA). Phase purity was confirmed by PXRD (Figure S2).

$[Cu^{II}(L)Cl]_2$: Yield: 35% (based on H*L*). Elemental analyses calc. (%) for $Cu_2(C_9H_9N_2O)_2Cl_2$ C, 41.55; H, 3.49; N, 10.77; Found (%): C, 41.60; H, 3.48; N, 10.80. Selected IR (KBr): 3444(s), 2893(w), 2838(w), 1633(m), 1491(m), 1454(m), 1316(w), 1088(m), 1003(s), 898(w), 745(m), 654(w), 484(w) cm^{-1} (Figure S3).

Crystallographic studies: Single-crystal X-ray diffraction data for **Cu2** at 296 and 90 K were collected on a Bruker Smart Apex CCD and an Agilent Supernova CCD diffractometer, respectively. Both employed graphite-monochromated Mo Kα radiation (λ = 0.71073 Å). The structure was solved by direct methods and refined by full-matrix least-squares method on F^2 using the SHELXTL program package.[21] All non-hydrogen atoms were refined with anisotropic displacement parameters. The F_o–F_c maps identified all the hydrogen atoms with electron densities higher than 2σ level. The crystal data are summarized in Table S1 of the Supporting information. Selected bond lengths and angles are listed in Table S2. CCDC 1585174 (**Cu2_90K**) and 1585175 (**Cu2_296K**) contain the supplementary crystallographic data for this paper. These data are provided free of charge by Cambridge Crystallographic Data Centre.

Mass Spectrometry Measurement: ESI-MS measurements were conducted at a capillary temperature of 275 °C. Aliquots of the solution were injected into the device at 0.05 mL/min. The mass spectrometer used for the measurements was a Thermo Exactive, and the data were collected in positive ion mode. The spectrometer was previously calibrated with the standard tune mix to give a precision of ca. 2 ppm in the region of 50−5000 *m/z*. The capillary voltage was 50 V, the tube lens voltage was 150 V, and the skimmer voltage was 25 V. The in-source energy was set to the range of 0−100 eV with a gas flow rate at 10% of the maximum. The crystals of **Cu2** were dissolved in DMSO and diluted with CH_3OH and the MS spectra were recorded in positive mode.

Computational Methodology: Complexation energies between $[Cu(HL)Cl]_2$ segments in the structure of **Cu2** and their possible direct-contact neighbors were calculated using B3LYP functional adding the D3 version of Grimme's dispersion with Becke-Johnson damping and SDD ECP for Cu and 6-311G(d) basis sets for other elements. These results make it possible to separate each interaction among the complex set of interaction energies within the crystal structures. The possible structures of the MS fragments were fully optimized using B3LYP functional with SDD ECP for Cu and 6-311G(d) basis set for other elements. At the optimized structures, harmonic vibrational frequencies (all real) were calculated to confirm that all optimized structures correspond to energy minima. Magnetic exchange interactions between Cu^{II} ions of **Cu2** were calculated using Noodleman's broken symmetry model based on geometry observed from single-crystal diffraction. All calculations were performed using Gaussian 16 software.[22]

Conflicts of interest

There are no conflicts to declare.

Acknowledgements

This work was supported by the National Science Foundation for Distinguished Young Scholars of China (No. 21525101), the NSF of Hubei and Guangxi Province (2017CFA006, 2017GXNSFDA198040), the BAGUI talent program (201904) and the Project of Talents Highland of Guangxi Province. M. K. is supported by CNRS-France.

Notes and references

1 (a) S. Datta, M. L. Saha and P. J. Stang, *Acc. Chem. Res.,* 2018, **51**, 2047–2063; (b) L. G. Christie, S. Asche, J. S. Mathieson, L. Vila, L. Cronin, *J. Am. Chem. Soc.*, 2018, **140**, 9379–9382; (c). Q.-M. Wang, Y.-M. Lin, K.-G. Liu, *Acc. Chem. Res.,* 2015, **48**, 1570–1579; (d) B. Liu, F. Yu, M. Tu, Z.-H. Zhu, Y. Zhang, Z.-W. Ouyang, Z. Wang and M.-H. Zeng, *Angew. Chem. Int. Ed.,* 2019, **58**, 3748–3753.

2 T. Shiga, J. Wang, J. Zhao, Z. Li, J. Dai, M. Damjanovic, H. Oshio, M. Yamashita and X. Bu, *Angew. Chem. Int. Ed.,* 2019, **58**, 4339–4344.

3 Z. Yin, Q.-X. Wang, M-H. Zeng, *J. Am. Chem. Soc.,* 2012, **134**, 4857−4863.

4 (a) Y. Yang, Q. Zhao, W. Feng, F. Li, *Chem. Rev.,* 2013, **113**, 192–270; (b) M. L. Saha, X. Yan, P. J. Stang, *Acc. Chem. Res.,* 2016, **49**, 2527–2539; (c) M.-H. Zeng, Z. Yin, Z.-H. Liu, H.-B. Xu, Y.-C. Feng, Y.-Q. Hu, L.-X. Chang, Y.-X. Zhang, J. Huang and M. Kurmoo, *Angew. Chem. Int. Ed.,* 2016, **55**, 11407–11411.

5 (a) D. Schröder, *Acc. Chem. Res.,* 2012, **45**, 1521–1532; (b) H. N. Miras, F. Wilson, L. Cronin, *Chem. Commun.,* 2009, 1297–1311; (c) W. Schrader, P. P. Handayani, J. Zhou, B. List, *Angew. Chem. Int. Ed.,* 2009, **48**, 1463–1466.

6 Q.-F. Sun, S. Sato, M. Fujita, *Nat. Chem.,* 2012, **4**, 330–333.

View Article Online
DOI: 10.1039/C9DT02890K

7 (a) Y.-Q. Hu, M.-H. Zeng, K. Zhang, S. Hu, F.-F. Zhou and M. Kurmoo, *J. Am. Chem. Soc.,* 2013, **135**, 7901–7908; (b) K. Zhang, M. Kurmoo, L.-Q. Wei and M.-H. Zeng, *Sci. Rep.,* 2013, **3**, 3516–3521.
8 X.-L. Chen, H.-B. Xu, X.-X. Shi, Y. Zhang, T. Yang, M. Kurmoo, M.-H. Zeng, *Inorg. Chem.,* 2017, **56**, 14069–14076.
9 H.-L. Zheng, X.-L. Chen, T. Li, Z. Yin, Y. Zhang, M. Kurmoo, M.-H. Zeng, *Chem. - Eur. J.,* 2018, **24**, 7906–7912.
10 X.-X. Shi, Y. Zhang, Q.-J. Chen, Z. Yin, X.-L. Chen, Z. Wang, Z.-W. Ouyang, M. Kurmoo, M.-H. Zeng, *Dalton Trans.,* 2017, **46**, 16663–16670.
11 M. Llunell, D. Casanova, J. Cirera, S. Alvarez, P. Alemany. Program for the Stereochemical Analysis of Molecular Fragments by Means of Continuous Shape Measures and Associated Tools. 2010, No. December, 30.
12 M.-H. Zeng, Y.-L. Zhou, W.-X. Zhang, M. Du, H.-L. Sun, *Cryst. Growth and Des.*, 2010, **10**, 20–24.
13 (a) Q. Li, Q.-H. Liu, W. Wei, Y.-Q. Zhang, S.-L. Liu, J.-M. Shi, *Z. Anorg. Allg. Chem.,* 2013, **639**, 181–186; (b) N. Robertson, P. Richardson, B. Roach, K. Awaga, F. J. White, D. K. Henderson, M. M. Matsushita, A. M. Whyte, P. A. Tasker, *Inorg. Chem.,* 2011, **50**, 12867–12876.
14 (a) M. K. Singh, G. Rajaraman, *Chem. - Eur. J.,* 2015, **21**, 980–983; (b) Y.-M. Jiang, Z. Yin, K.-H. He, M.-H. Zeng, M. Kurmoo, *Inorg. Chem.,* 2011, **50**, 2329–2333.
15 S. E. Wheeler, *Acc. Chem. Res.,* 2013, **46**, 1029–1038.
16 Z. Han, G. Zhang, M. Zeng, D. Yuan, Q. Fang, J. Li, *Inorg. Chem.,* 2010, **49**, 769–771.
17 (a) L. Noodleman, *J. Chem. Phys.*, 1981, **74**, 5737–5743; (b) L. Noodleman, D. A. Case, A. Aizman, *J. Am. Chem. Soc.,* 1988, **110**, 1001–1005.
18 (a) J. Wang, Y.-F. Wu, M. Kurmoo, M.-H. Zeng, *Inorg. Chem*., 2019, **58**, 7472-7479; (b) L.-Y. Guo, H.-F. Su, M. Kurmoo, C.-H. Tung, D. Sun, L.-S. Zheng, *J. Am. Chem. Soc*., 2017, **139**, 14033–14036.
19 (a) M. Handa, N. Koga, S. Kida, *Bull. Chem. Soc. Jpn.*, 1988, **61**, 3853–3857; (b) C. A. Bear, J. M. Waters, T. N. Waters, *J. Chem. Soc., Dalton Trans.*, 1974, 1059–1062; (c) M. Zhang, D.-M. Xian, N. Zhang, H.-H. Li, Z.-L. You, *Struct. Chem.*, 2012, **23**, 1489–1496; (d) N. Lah, I. Leban, R. Clérac, *Eur. J. Inorg. Chem.,* 2006, **2**, 4888–4894; (e) C. Fukuhara, K. Tsuneyoshi, K. Katsura, N. Matsumoto, S. Kida, M. Mori, *Bull. Chem. Soc. Jpn.*, 1989. **62**. 3939–3943.
20 Mercury 3.9, Cambridge Crystallographic Data Centre (CCDC).
21 (a) G. M. Sheldrick, *Acta Crystallogr., Sect. A: Found. Crystallogr,* 2008, **64**, 112−122; (b) G. M. Sheldrick, *Acta Crystallogr., Sect. C: Struct. Chem,* 2015, **71**, 3−8.
22 Gaussian 16, Revision A.03, M. J. Frisch, G. W. Trucks, H. B. Schlegel, G. E. Scuseria, M. A. Robb, J. R. Cheeseman, G. Scalmani, V. Barone, G. A. Petersson, H. Nakatsuji, X. Li, M. Caricato, A. Marenich, J. Bloino, B. G. Janesko, R. Gomperts, B. Mennucci, H. P. Hratchian, J. V. Ortiz, A. F. Izmaylov, J. L. Sonnenberg, D. Williams-Young, F. Ding, F. Lipparini, F. Egidi, J. Goings, B. Peng, A. Petrone, T. Henderson, D. Ranasinghe, V. G. Zakrzewski, J. Gao, N. Rega, G. Zheng, W. Liang, M. Hada, M. Ehara, K. Toyota, R. Fukuda, J. Hasegawa, M. Ishida, T. Nakajima, Y. Honda, O. Kitao, H. Nakai, T. Vreven, K. Throssell, J. A. Montgomery, Jr., J. E. Peralta, F. Ogliaro, M. Bearpark, J. J. Heyd, E. Brothers, K. N. Kudin, V. N. Staroverov, T. Keith, R. Kobayashi, J. Normand, K. Raghavachari, A. Rendell, J. C. Burant, S. S. Iyengar, J. Tomasi, M. Cossi, J. M. Millam, M. Klene, C. Adamo, R. Cammi, J. W. Ochterski, R. L. Martin, K. Morokuma, O. Farkas, J. B. Foresman, D. J. Fox, Gaussian, Inc., Wallingford CT, 2016.

View Article Online
DOI: 10.1039/C9DT02890K

Journal Name

ARTICLE

TOC

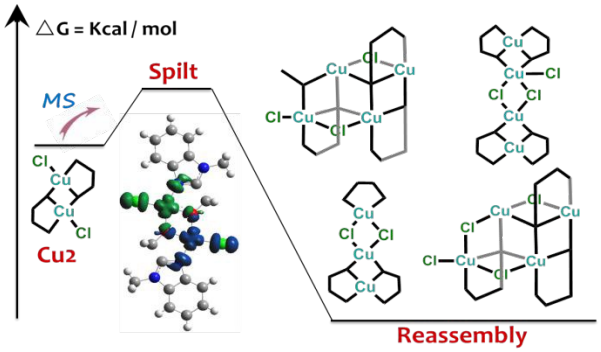

The flat binuclear $[Cu_2(L)_2Cl_2]$ (H*L* = 1-methyl-1H-benzo[d]imidazole-2-yl)methanol) was studied by single crystal mass spectrometry under difference in-source energies. Meanwhile its strong antiferromagnetism is characterized by g = 2.20, J = -465 cm^{-1} and zj = -0.83 cm^{-1} and these were substantiated by DFT calculations.